

Performance of Pile–Wall System Adjacent to Footings

Ghassan A. Sudani ^{1,*} and Mien Jao ^{2,*}¹ Independent Researcher, West Chester, OH 45069, USA² Department of Civil and Environmental Engineering, Lamar University, 4400 MLK Blvd., Beaumont, TX 77710, USA

* Correspondence: dr.ghassan.sudani@gmail.com (G.A.S.); mien.jao@lamar.edu (M.J.)

Abstract: The performance of a retaining wall is dependent on multiple factors including lateral earth pressure, which results from backfill soils and adjacent footings located behind a retaining wall. The prediction of a retaining wall's performance in a footing–soil–wall system (FSPS) must incorporate the influences caused by the movement of a retaining wall. This study examines the performance of a retaining wall formed by driven, precast, concrete piles located adjacent to a concrete footing using two- and three-dimensional finite element analysis (2D and 3D FEA) by ANSYS 13.0 software. Both soil and concrete are assumed to behave as non-linear, elastic-perfectly plastic and rate-independent materials in compliance with the upper-bound model of Drucker–Prager yield criterion. Three backfill and foundation soils are considered: kaolin, silty clay, and kaolin–sand. Various conditions of soil type, footing shape ratio, pile width, and footing–pile distance through 180 FEA runs are investigated. The effects of 2D and 3D FEA on the behavior of the pile–wall system are compared. The lateral deflection and pressure distribution profiles along the pile–wall are studied and presented. Two empirical equations predicting lateral deflections at the pile toe and pile head and useful for pile structural design are developed under the ultimate pressure of the adjacent footing.

Keywords: 3D non-linear finite element analysis; soil–structure interaction; retaining structures; footings; wall lateral displacement



Citation: Sudani, G.A.; Jao, M. Performance of Pile–Wall System Adjacent to Footings. *Appl. Sci.* **2024**, *14*, 3496. <https://doi.org/10.3390/app14083496>

Academic Editor: José António Correia

Received: 25 February 2024

Revised: 11 April 2024

Accepted: 19 April 2024

Published: 21 April 2024



Copyright: © 2024 by the authors. Licensee MDPI, Basel, Switzerland. This article is an open access article distributed under the terms and conditions of the Creative Commons Attribution (CC BY) license (<https://creativecommons.org/licenses/by/4.0/>).

1. Introduction

Several theories of lateral earth pressure acting on retaining walls and based on the classical theories of Coulomb [1] and Rankine [2] are currently used. Coulomb's theory [1], taking into account the friction at the wall–soil interface, is considered a more realistic model than Rankine's theory [2]. However, Coulomb did not cover the passive earth pressure, but later, Coulomb's theory was used by others to develop a formula for the passive earth pressure [3]. Bell [4] incorporated the cohesion factor of cohesive soils in the computations of lateral earth pressure. Terzaghi and Peck [5] developed a presumptive and conservative earth pressure model using the soil classification and the observed performance of real walls. However, for the stability of walls, Goh et al. [6] indicated that the exact distribution of earth pressure at the lower portion of a retaining wall is not easily determined due to the presence of passive earth pressure in front of the wall and, if any wall rotation, at the wall back.

According to the classification of earth-retaining structures by O'Rourke and Jones [7], a pile–wall is considered to act as an in situ, cantilevered wall of an externally stabilized system, and based on Coduto [3], the pile–wall depends on its flexural stiffness and embedment length to resist the lateral earth pressure without any additional supports. Goh et al. [6] indicated that the embedment length of a cantilevered wall is considered critical for wall design and concluded that the soil type, retained soil height, and loading configuration have significant impact on wall behavior. Teng [8] and Das [9] described an alternative conventional method to calculate the embedment length of a cantilevered wall. This conventional method simplifies the active and passive earth pressures acting on

a wall to net pressures with the equilibrium of moments and forces. For practical use, a conservative factor of safety is applied with this approach to either reduce the coefficient of passive earth pressure or increase the embedment length of the wall. Coduto [3] suggested that a pile is deemed to be long when its embedment length is greater than 35 times its diameter or width. For the inter-dependent effects between a pile–wall and a sloped backfill, Li [10] pointed out that the lateral pressure acting on the piles depends on factors, such as pile lateral capacity, pile flexural deformation, and the relative displacement between pile and soil. Duncan et al. [11] observed that the lateral earth pressure behind a retaining structure is non-linearly or curved distributed due to the soil arching phenomena caused by the large displacement of the retaining structure. By the classical theories and for a cohesionless backfill soil, the resultant force of lateral earth pressure acts at the lower one-third point of the embedded part of a retaining structure due to the assumption of linearly distributed earth pressure. In contrast to the results predicted by the classical theories, Handy [12] reported that the resultant force acts at 40% to 45% of the embedded part of a retaining structure from the bottom due to the soil-arching phenomena. As a result of this soil-arching phenomena, the classical solutions are not always conservative. Jiang et al. [13] later related the cause of the soil-arching phenomena to the non-homogeneous displacement in soil that causes stress release and particle rearrangement.

Coduto [3] stated that a retaining structure is significantly influenced by an adjacent surcharge load applied at a distance less than the exposed height of a retaining structure. Jarquio [14] proposed a solution using the elastic theory of Boussinesq to estimate the lateral pressure induced by an adjacent strip surface load on both flexible and rigid retaining walls. However, Jarquio’s solution results in greater lateral pressure due to a lack of consideration of soil properties and wall stiffness and movement [14]. In addition, Smith and Smith [15] stated that a reduction in the lateral pressures takes place due to changing the state of soil from an at-rest to an active condition caused by retaining wall movement. Wang et al. [16] and Dang et al. [17] pointed out that the current methods computing earth pressure have some limitations due to a lack of consideration of the impact of retaining wall displacement.

El Sawwaf [18] observed that the lateral capacity of a pile–wall nearby a strip footing is improved by decreasing the pile spacing and increasing pile embedment length and diameter. Sudani [19] indicated that the distance between a footing and a pile–wall has a significant impact on the footing bearing capacity. Sudani et al. [20] formulated an equation, as shown in Equation (1) below, to describe the effects of footing width, B_f , footing length, L_f , and internal friction angle of soil, ϕ , on the footing–wall critical distance, B_{cr} . Therefore, a footing does not interact with a pile–wall located beyond the footing–wall critical distance, B_{cr} .

$$\frac{B_{cr}}{B_f} = \sqrt[5]{1875 + 1.995 \left(\frac{L_f}{B_f}\right)^5 + 107729(\tan\phi)^5} \quad (1)$$

Jao et al. [21] pointed out that the degree of interaction between a strip footing and a sheet pile–wall is greatly dependent on the footing location and wall thickness, where the footing and wall displacements and wall lateral earth pressure increase while the ultimate bearing capacity of adjacent footing decreases. Aparna and Samadhiya [22] indicated, based on an experimental study, that the performance of a sheet pile–wall adjacent to a footing is substantially influenced by the footing distance to the sheet pile–wall. Azzam and Elwakil [23] studied the behavior of an axially loaded–piled retaining wall where the ultimate axial capacity of the tested pile–wall was significantly increased with the increase in soil relative density and wall-penetration depth. In addition, the lateral wall deformation and maximum bending moment with the ultimate axial capacity were considerably reduced by 50% due to the existence of surcharge stress within the active zone behind the piled retaining wall in accordance with their results.

Ter-Martirosyan and Vanina [24] analyzed the effect of the load from stockpiled materials and construction machinery near the edge of a rectangular retaining wall on a soil

foundation resting on an incompressible base. Their analyses indicated that the displacement of horizontal stresses toward a retaining wall results in extra internal forces in the retaining wall, which should be considered for reinforcing concrete retaining walls. They also pointed out that there are still no theoretical solutions considering a large range of factors forming the stress–strain statement of a soil basis, the distance of the building from the pit, the load on the foundation, and the width and length of the foundation. Fan et al. [25] studied embedded cantilever retaining walls (piles) by considering the displacement control of walls and reported that the wall rotation point is located in proximity to the wall base. They concluded that, in spite of research being conducted for the deformation control design of an embedded cantilever retaining pile–wall, a realistic and simple-to-use design method to determine the required embedment depth based on the deformation control is still to be investigated. Eilat et al. [26] numerically investigated embedded walls by using a database of actual wall movements. They observed that the wall bending moments are greater and increase with wall height based on analytical calculations and, therefore, an accurate prediction of wall deflections remains a significant engineering challenge.

In light of the literature findings, it is clear that predicting the behavior of a retaining wall using classical solutions is not sufficient under the effects of adjacent footing pressure and wall flexibility and movement. In addition, the behavior of a retaining wall formed of piles that interact with adjacent footings of different shape ratios on various soil types cannot be explained by the traditional approaches. In this study, the profiles of lateral pressure and deflection of pre-embedded pile–walls influenced by multiple factors, such as soil type, footing shape ratio, footing–pile distance, and pile width, are systematically investigated. This investigation is completed using the finite element analysis (FEA) software package of ANSYS 13.0 [27] through 180 runs of various conditions and eleven unique cases to rank the factors influencing the performance of a pile–wall system. The results are used to develop a safer and more realistic solution and facilitate practically the geotechnical and structural design of a pile–wall system.

2. Numerical Model

The concrete and soil in a footing–soil–pile system (FSPS) are idealized as non-linear, elastic-perfectly plastic and rate-independent materials obeying the upper-bound yield criterion of Drucker–Prager [28]. Two- and three-dimensional finite element (2D and 3D FE) models for FSPS are generated by the FEA software package of ANSYS 13.0 [27]. The following assumptions are made for the 2D and 3D FE models: (1) pile–walls interacting with adjacent embedded footings supporting uniformly distributed pressures; (2) soils having homogeneous and isotropic mediums; (3) no impacts of consolidation and creep on the behavior of pile–walls and footings; and (4) no influence of the ground water table on the stress–strain behavior of soils.

The schematic view and sections of the 2D and 3D FE models of FSPS are shown in Figure 1. Figure 1a–d show the schematic top view, the transverse section at the pile–wall location, the longitudinal section at the symmetrical axis, and the transverse section at the footing location, respectively, with the side, out-of-plane, and bottom boundaries for the 3D FE model of FSPS. In addition, Figure 1c depicts the schematic view with the side and bottom boundaries for the 2D FE model of FSPS. The boundary conditions shown in Figure 1 are (1) side boundaries restricted from displacing in the x-direction; (2) bottom boundaries restricted from displacing in the x-, y-, and z-directions; and (3) out-of-plane boundaries restricted from displacing in the z-direction. Sudani et al. [20] demonstrated that the locations of these boundaries, which are the result of a non-dimensional parametric study by a trial-and-error procedure, have a negligible impact on the behavior of an FSPS. In addition, Sudani et al. [20] validated the FSPS boundaries used in this study for kaolin, silty clay, and kaolin–sand soils using previous experimental tests conducted by Badie [29], Baus [30], and Azam [31], respectively.

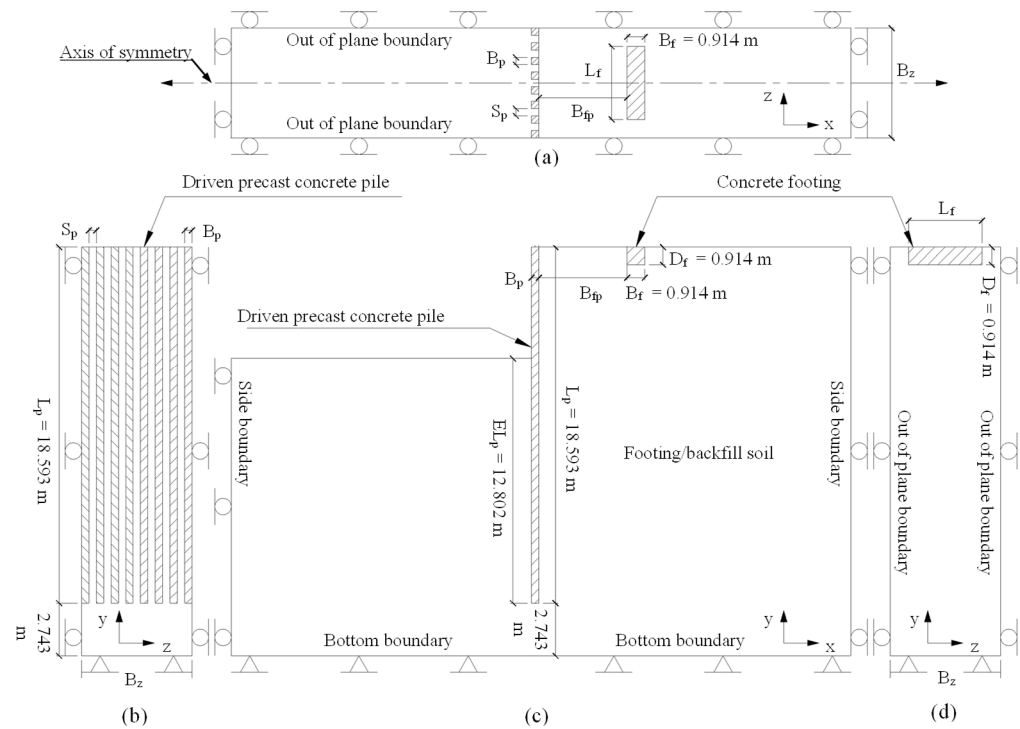


Figure 1. Schematic view, sections, and boundaries for 2D and 3D FE models of FSPS: (a) top view of 3D FE model with side and out-of-plane boundaries; (b) transverse section at pile–wall location of 3D FE model with out-of-plane and bottom boundaries; (c) longitudinal section at symmetrical axis of 3D FE model and schematic view of 2D FE model with side and bottom boundaries; and (d) transverse section at footing location of 3D FE model with out-of-plane and bottom boundaries. Reprinted/adapted with permission from Ref. [20]. 2024, American Society of Civil Engineers.

The schematic view and sections of the 2D and 3D FE models shown in Figure 1 are meshed with linear finite elements having elastic, plastic, and large strain capabilities, as demonstrated in Figure 2. The quadrilateral four-node linear element (PLANE42) is selected for the plane strain analysis of the 2D FE model. The hexahedron eight-node linear element (SOLID45) is chosen for the analysis of the 3D FE model. The initial conditions of the geostatic or at-rest condition stresses governed by gravity and density are set for the 2D and 3D FE models ahead of the analysis.

Three backfill/footing soils are considered in this study: kaolin, silty clay, and kaolin–sand. The properties of kaolin, silty clay, and kaolin–sand soils were studied by Baus and Wang [32], Badie and Wang [33], and Azam et al. [34], respectively. The strength properties of the backfill/footing soils, which are the result of a test of triaxial compression consolidated drained (CD), are applicable for the long-term condition. The concrete of the piles and footings is chosen with mechanical properties studied by Azam [35]. For a smooth concrete face, Bowles [36] recommended a friction angle at the soil–concrete interface, ϕ_{sc} , between 60% and 80% of the soil internal friction angle ϕ . Therefore, the friction angle at the soil–concrete interface is selected as 70% of the soil internal friction angle. The properties of the backfill/footing soils and concrete for the FSPS are tabulated in Table 1.

The width, B_f , and depth, D_f , of the footing are selected to be constant at 0.914 m. The driven concrete pile is chosen to have a square section with three different pile widths, B_p : 0.254, 0.305, and 0.356 m. The total length, L_p , and embedment length, EL_p , of the pile are decided to be 18.593 and 12.802 m, respectively. From these geometries of the pile, the pile is defined as a long pile with a ratio of embedment length to width greater than 35, as indicated by Coduto [3]. The depth of the 3D FE model in the z - or out-of-plane direction is set to be 15 times the width of the pile. Sudani et al. [20] confirmed that this depth of

the 3D FE model enclosed by the out-of-plane boundaries has a negligible impact on the behavior of the FSPS. The above constant parameters of the FSPS are shown in Figure 1.

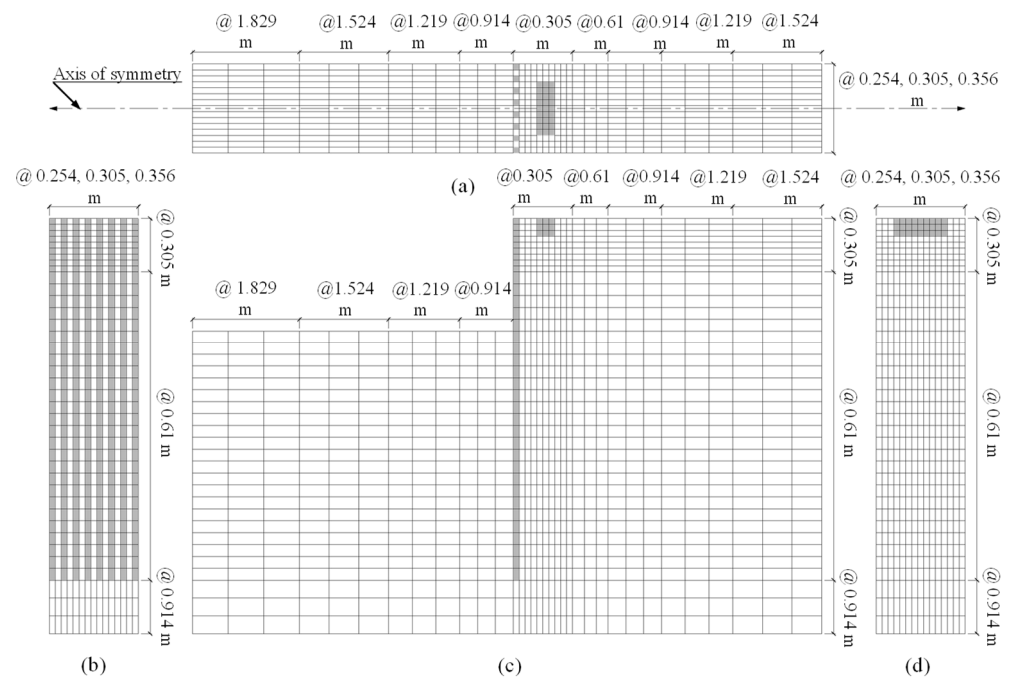


Figure 2. Schematic view and sections of mesh for 2D and 3D FE models of FSPS showing the finite element sizes: (a) top view of 3D FE model; (b) transverse section at pile–wall location of 3D FE model; (c) longitudinal section at symmetrical axis of 3D FE model and schematic view of 2D FE model; and (d) transverse section at footing location of 3D FE model. Reprinted/adapted with permission from Ref. [20]. 2024, American Society of Civil Engineers.

Table 1. Properties of backfill/footing soils and concrete for the FSPS.

Properties	Kaolin	Silty Clay	Kaolin–Sand	Concrete
Initial modulus in compression E_i (kN/m ²)	19,843	4670	42,029	22.7×10^6
Poisson’s ratio ν	0.39	0.28	0.32	0.2
Wet unit weight γ (kN/m ³)	16.7	18.4	18.5	24.39
Unit cohesion c (kN/m ²)	158.5	65.5	9.2	7235
Water content ω	23%	17%	11.8%	-
Internal friction angle ϕ deg.	8.0	13.5	31.0	20.0
Friction angle at soil–concrete interface ϕ_{sc} , (deg.)	5.6	9.5	21.7	-

The variables of the FSPS are investigated with a wide range into 180 combinations of different conditions. Three different soil types are used: kaolin, silty clay, and kaolin–sand. Four footing shape ratios (L_f/B_f) are selected: 1, 2, 3, and 5/infinite. Four footing–pile distances (B_{fp} face to face) are chosen: 0.914, 2.743, 4.572, and 6.401 m; three pile widths (B_p), which are equal to the pile-to-pile spacings (S_p), are studied: 0.254, 0.305, and 0.356 m. The variables and conditions considered for the FSPS in this study are tabulated in Table 2. Som and Das [37] referred to the factors affecting the pile-to-pile spacing, such as soil type, installation method, layout and verticality errors, pile group efficiency, and economy. Tomlinson and Woodward [38] stated a recommendation that the spacing between adjacent piles must not be less than the smallest width of the pile. Therefore, the pile spacing (S_p) is selected to be equal to the pile width (B_p).

Table 2. Variables and conditions of FSPS.

Variable	Description/Value	No. of Conditions
Analysis Type	2D plane strain and 3D FEA	2
Soil Type	Kaolin, silty clay, and kaolin–sand	3
L_f/B_f	1, 2, 3, and 5/infinite	1 and 4 for 2D and 3D FEA, respectively
B_{fp}/B_f	1, 3, 5, and 7	4
B_p and S_p (m)	0.254, 0.305, and 0.356	3
Total No. of Conditions		180

Currently, experimental tests for FSPS are not available. However, the present 3D FE models of the FSPS were validated with previous experimental tests performed for systems of footing–soil by Badie [29], Baus [30], and Azam [31] for kaolin, silty clay, and kaolin–sand, respectively. When the footing is located outside the footing–wall critical distance, where the performance of the adjacent pile–wall is not affected by the footing, the FSPS behaves as the footing–soil system. For this validation, the 3D FE models and experimental tests utilized surface strip footings of 0.051 m width resting on the three different soils of kaolin, silty clay, and kaolin–sand. The present validation, depending on the footing pressure–settlement (P – δ_v) curves as shown in Figure 3, exhibits a good agreement regarding the results of the 3D FE models and previous experimental tests. The most differences among the results of the present validation are as follows: 21.6% for kaolin in Figure 3a; 13.8% for silty clay in Figure 3b; and 18.7% for kaolin–sand in Figure 3c.

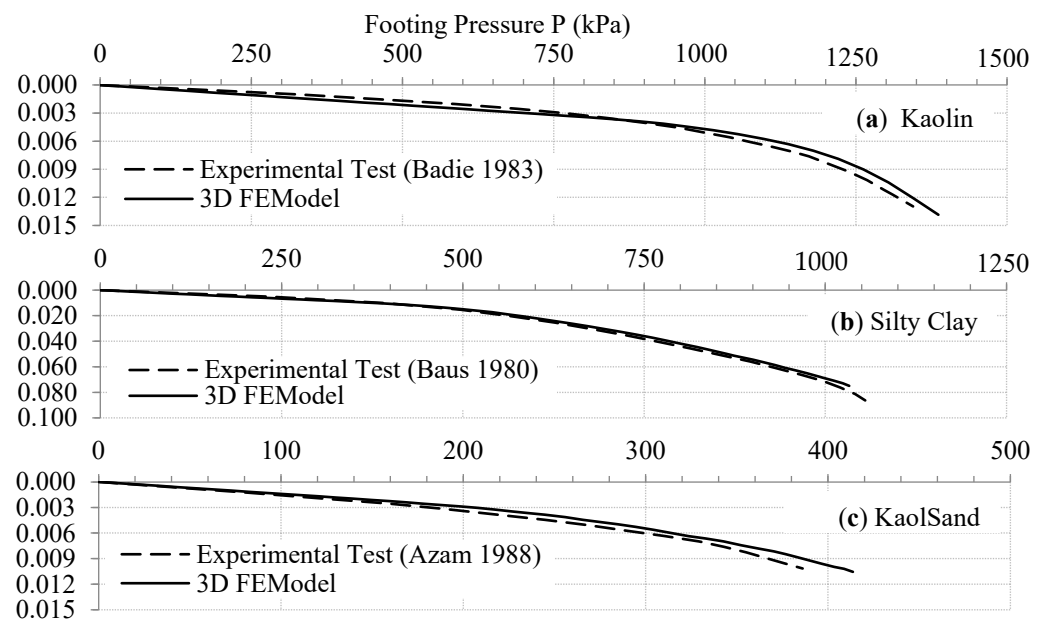


Figure 3. Validation of P – δ_v curves resulting from 3D FE models with previous experimental tests for surface strip footings without adjacent pile–walls resting on (a) kaolin [29]; (b) silty clay [30]; and (c) kaolin–sand [31]. Reprinted/adapted with permission from Ref. [20]. 2024, American Society of Civil Engineers.

3. Comparison of Two- and Three-Dimensional Finite Element Analyses

Two-dimensional (plane strain) finite element analysis (2D FEA) may not provide an accurate response of a FSPS, particularly for a footing with a small shape ratio (square footing) adjacent to a wall of spaced piles (pile–wall), because of the limitations in considering the square footing and pile–wall as a continuous (infinite shape ratio) footing and wall. The effects of out-of-plane geometries (footing length and pile spacing) of this FSPS can be modeled more appropriately using three-dimensional finite element analysis (3D FEA).

The profiles of pile lateral deflection (δ_L) versus depth for a pile–wall adjacent to a square footing, which is under a pressure (P) of 200 kPa and resting on kaolin–sand soil, are shown in Figure 4 using 2D and 3D FEA. Pile deflections are measured along the middle pile of the pile–wall and at its center shown as point 1 in Figure 1c. Figure 4 shows that the pile is shifted and deflected, and the pile deflections in 2D and 3D FEA have a similar trend below a depth of 8.0 m, but they diverge above a depth of 8.0 m. In addition, Figure 4 shows that the lateral deflection of the pile head (δ_{LH}) using 2D FEA is 0.0315 m, which is 450% greater than the 0.007 m of δ_{LH} using 3D FEA. The divergence between the pile deflections is mainly because the square footing in 2D FEA is treated as a continuous/infinite footing, which induces greater lateral pressure on the pile–wall. Due to the soil support in front of the pile–wall, as shown in Figure 1c, the deflection profiles of 2D and 3D FEA are bent between the depths of 5.0 and 8.0 m. Below a depth of 8 m, the two profiles of pile deflections are approximately merged together. The change in the shape ratio for the footing and/or pile spacing for the pile–wall has a negligible impact on the pile deflection below a depth of 8.0 m. The lateral deflections of the pile toe (δ_{LT}) using both 2D and 3D FEA have an approximately identical deflection at 0.0015 m, indicating a small influence from the adjacent footing pressure and an identical point of pile fixity.

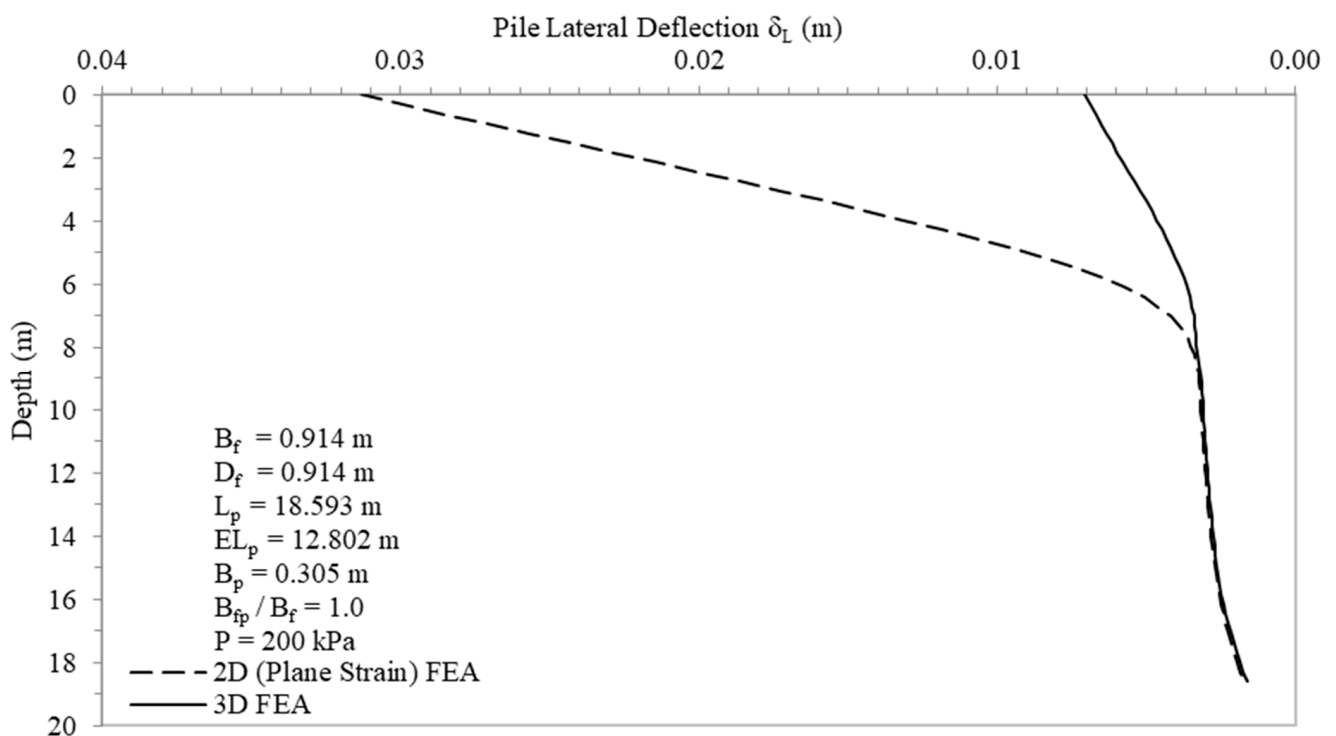


Figure 4. δ_L versus depth profiles of pile–wall adjacent to square footing resting on kaolin–sand soil.

From the comparisons in Figure 4 for a pile–wall adjacent to a square footing, it is clear that 2D FEA in comparison with 3D FEA may underestimate the pile lateral deflection by more than 400% because 2D FEA cannot consider the footing shape ratio and pile spacing.

4. Parametric Study

A sample of eleven cases of different conditions, as tabulated in Table 3, is chosen to show the influence of the variables considered in this study on the behavior of a pile–wall. Cases (a), (b), (c), and (d) are utilized to show the influences of pile width (B_p) and footing–pile distance (B_{fp}) on the lateral deflections and pressures of a pile–wall. Cases (e), (f), (g), and (h) are used to show the effects of the footing shape ratio (L_f/B_f) and footing–pile distance (B_{fp}) on the lateral deflections and pressures of a pile–wall. Cases (f), (k), (m), and (n) are employed to show the impacts of soil type on the lateral deflections and pressures

of a pile–wall. The behavior of a pile–wall is investigated through observing the profiles of pile lateral deflection and pressure versus pile depth.

Table 3. Sample of different cases for footing–soil–pile system.

Case	Soil	P (kPa)	B_p (m)	B_{fp}/B_f	L_f/B_f
(a)	Kaolin	1027	0.254	1	Strip footing (infinite shape ratio)
(b)	Kaolin	1027	0.254	3	Strip footing (infinite shape ratio)
(c)	Kaolin	1027	0.356	1	Strip footing (infinite shape ratio)
(d)	Kaolin	1027	0.356	3	Strip footing (infinite shape ratio)
(e)	Kaolin	1027	0.254	1	Rectangle footing (shape ratio 3.0)
(f)	Kaolin	1027	0.254	1	Square footing (shape ratio 1.0)
(g)	Kaolin	1027	0.254	3	Rectangle footing (shape ratio 3.0)
(h)	Kaolin	1027	0.254	3	Square footing (shape ratio 1.0)
(k)	Silty clay	1027	0.254	1	Square footing (shape ratio 1.0)
(m)	Silty clay	400	0.254	5	Square footing (shape ratio 1.0)
(n)	Kaolin–sand	400	0.254	5	Square footing (shape ratio 1.0)

The profiles of pile lateral deflection (δ_L) versus depth for pile–walls adjacent to strip footings, which are resting on kaolin soil and loaded by a pressure (P) of 1,027 kPa, are shown in Figure 5. This figure presents the first four cases shown in Table 3, (a), (b), (c), and (d), to observe the influence of pile width (B_p) and footing–pile distance (B_{fp}) on pile lateral deflections.

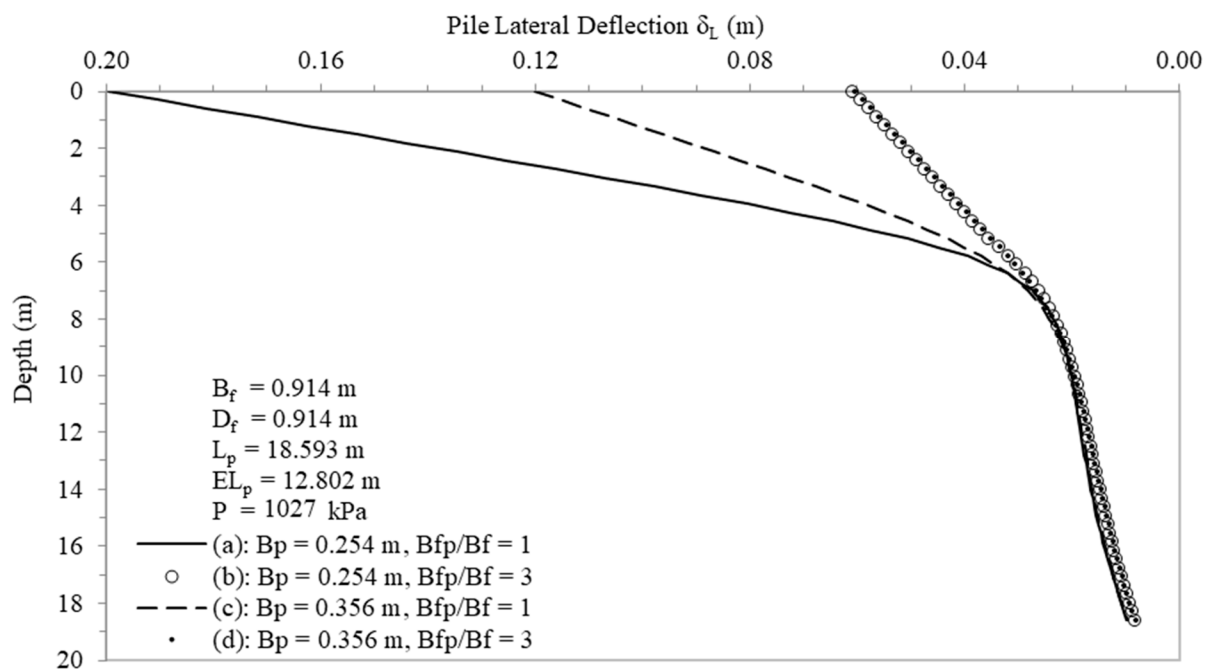


Figure 5. δ_L versus depth profiles of pile–wall adjacent to strip footings resting on kaolin soil.

It is clear that the piles move approximately an equal lateral displacement (δ_{LT}) of 0.008 m at their toes, which shows a very small influence of pile width (B_p) and footing–pile distance (B_{fp}) on the pile toe deflection. The amount of pile head lateral deflection (δ_{LH}) depends on the pile width (B_p) and footing–pile distance (B_{fp}). Similar to Figure 4, the deflection profiles are bent between depths of 5.0 and 8.0 m. The divergence of deflection profiles above a 7.0 m depth shows the great influence of the adjacent footing on pile deflection, while below a 7.0 m depth, the approximately merged profiles show little influence of the adjacent footing on pile deflection. For a constant footing–pile distance (B_{fp}) of 0.914 m in cases (a) and (c) and between depths of 0.0 and 7.0 m of Figure 5, the pile

deflections show a significant effect of increasing pile width (B_p) from 0.254 to 0.356 m on decreasing the pile head deflection from 0.2 to 0.12 m. For a constant pile width (B_p) of 0.254 m in cases (a) and (b) of Figure 5, the increase in footing–pile distance (B_{fp}) from 0.914 to 2.742 m shows a greater impact than pile width (B_p) on decreasing the pile head deflection from 0.2 to 0.06 m. For a constant footing–pile distance (B_{fp}) of 2.742 m in cases (b) and (d) of Figure 5, the increase in pile width (B_p) from 0.254 to 0.356 m shows a very small impact on the pile deflection, which reveals that, when footing–pile distance increases, the influence of pile width on the pile deflection decreases. For a constant pile width (B_p) of 0.356 m in cases (c) and (d) of Figure 5, the increase in footing–pile distance (B_{fp}) from 0.914 to 2.742 m shows a significant impact on decreasing the pile head deflection from 0.12 to 0.06 m.

The profiles of pile lateral deflection (δ_L) versus depth for a constant pile width (B_p) of 0.254 m adjacent to rectangle and square footings, which are resting on kaolin soil and loaded by a pressure (P) of 1027 kPa, are shown in Figure 6. This figure presents the second four cases shown in Table 3, (e), (f), (g), and (h), to investigate the effects of footing shape ratio (L_f/B_f) and footing–pile distance (B_{fp}) on the deflection profile.

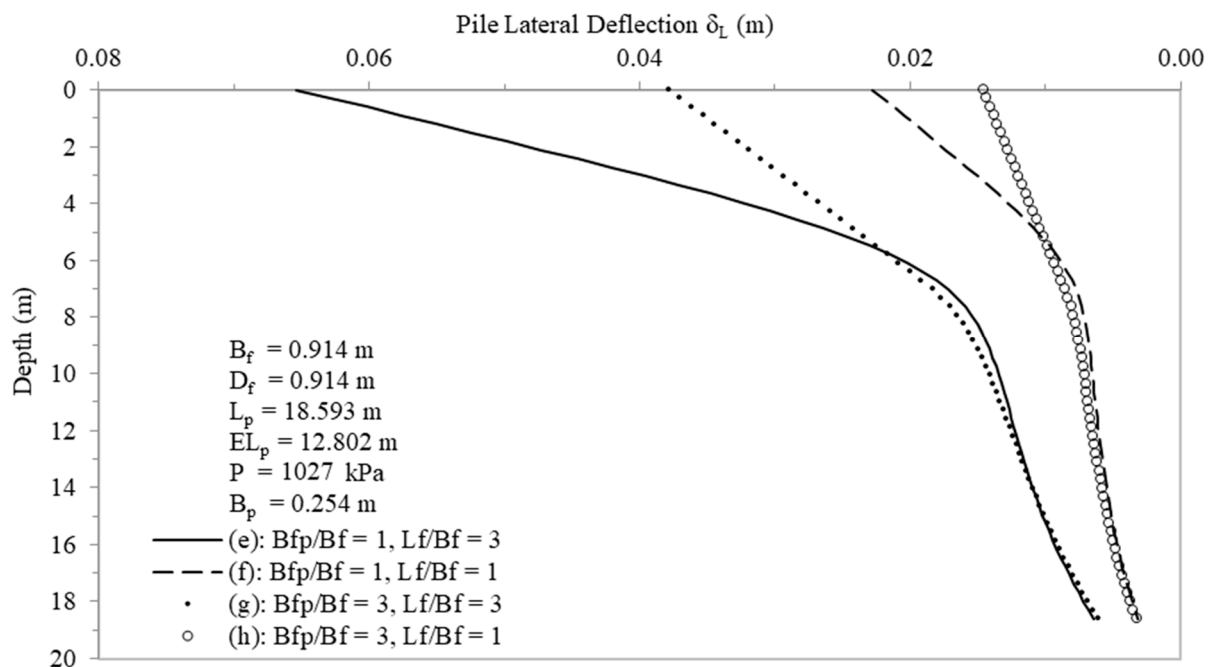


Figure 6. δ_L versus depth profiles of pile–wall adjacent to rectangle and square footings resting on kaolin soil.

For a rectangle footing with a shape ratio (L_f/B_f) of 3 in cases (e) and (g) of Figure 6, the pile deflections show a significant impact of increasing footing–pile distance (B_{fp}) from 0.914 to 2.742 m on decreasing the pile head deflection from 0.063 to 0.038 m, but it shows a small impact on the pile toe deflection. For a constant footing–pile distance (B_{fp}) of 0.914 m in cases (e) and (f) of Figure 6, the decrease in footing shape ratio (L_f/B_f) from 3 (rectangle) to 1 (square) shows a greater effect than footing–pile distance (B_{fp}) on decreasing the pile deflection from 0.063 to 0.023 m at its head and from 0.006 to 0.003 m at its toe. For a square footing with a shape ratio (L_f/B_f) of 1.0 in cases (f) and (h) of Figure 6, the increase in footing–pile distance (B_{fp}) from 0.914 to 2.742 m shows a significant influence on decreasing the pile deflection from 0.023 to 0.014 m at its head, but it shows no influence on the pile toe deflection. For a constant footing–pile distance (B_{fp}) of 2.742 m in cases (g) and (h) of Figure 6, the decrease in footing shape ratio (L_f/B_f) from 3 (rectangle) to 1 (square) shows a great impact on decreasing the pile deflection from 0.038 to 0.014 m at its head and from 0.006 to 0.003 m at its toe.

Based upon the pile toe deflections from the different cases in Figures 5 and 6, the pile toe deflection is independent of the footing–pile distance (B_{fp}) and pile width (B_p) but particularly sensitive to the footing shape ratio (L_f/B_f), as shown in Figure 6. This conclusion can be explained by the influence of induced pressure, which is proportional to the footing shape ratio, i.e., the bigger the footing shape ratio is, the greater the pressure is induced at a deeper depth. In addition, the independency of pile toe deflection from the footing–pile distance and pile width is an advantage of using the long piles in this study.

The profiles of pile lateral deflection (δ_L) versus depth for a constant pile width (B_p) of 0.254 m adjacent to square footings, which are resting on silty clay and kaolin–sand soils, are shown in Figure 7. This figure presents the last three cases shown in Table 3, (k), (m), and (n), to study the impact of soil type on the deflection profile.

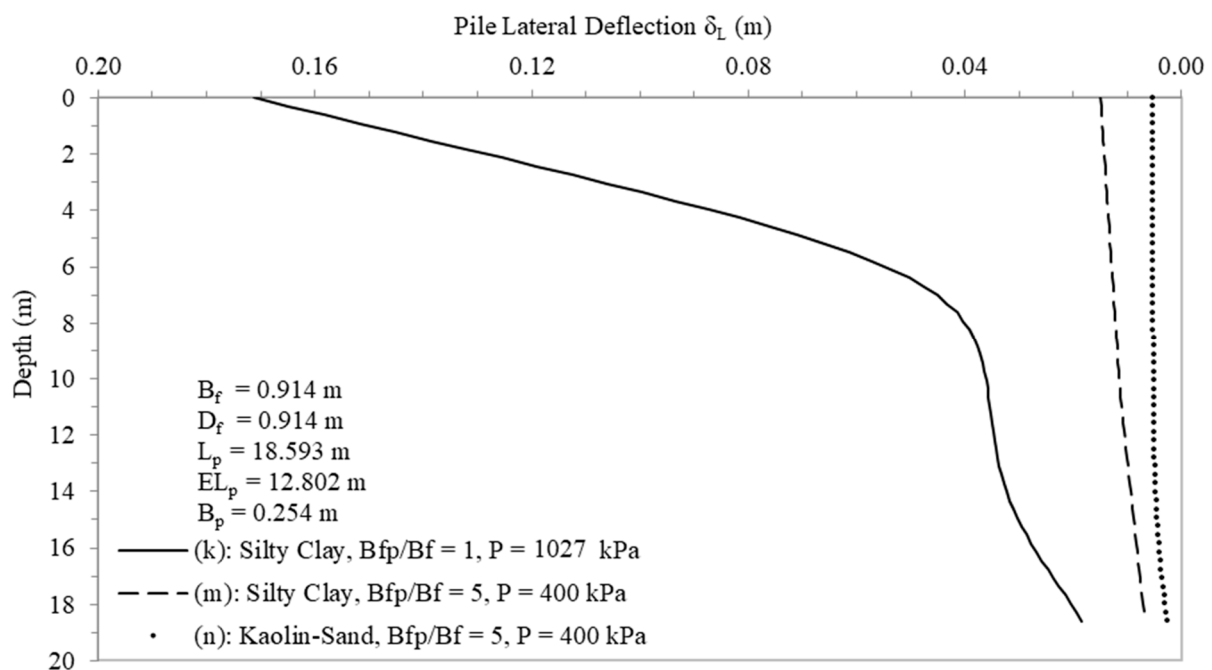


Figure 7. δ_L versus depth profiles of pile–wall adjacent to square footings resting on silty clay and kaolin–sand soils.

The pile deflection profiles vary with respect to the change in soil type, footing–pile distance, and footing pressure. For a square footing (shape ratio of 1) at a constant footing–pile distance (B_{fp}) of 4.57 m and under footing pressure (P) of 400 kPa in cases (m) and (n) of Figure 7, the change in soil from silty clay to kaolin–sand shows a significant impact on reducing the pile deflections from 0.016 to 0.006 m at its head and from 0.006 to 0.002 m at its toe. In addition, greater impact is observed from changing the soil type from silty clay in Figure 7 (k) to kaolin in Figure 6 (f), where pile deflections are reduced from 0.172 to 0.023 m at its head and from 0.018 to 0.003 m at its toe. The significant reduction in pile deflection due to the change in soil type from silty clay to kaolin and silty clay to kaolin–sand is related to the initial modulus in compression (E_i), shown in Table 1, where kaolin–sand and kaolin have higher moduli in compression than silty clay.

Based on the profiles of pile deflection in Figures 5–7, the behavior of bent piles confirms that the piles are long, which are chosen based upon the pile embedment length to pile width ratio of greater than 35, which is stated by Coduto [3]. Also, the pile bending between depths of approximately 5.0 and 8.0 m is mainly related to the pile embedment length, where the other variables of soil type, footing shape ratio, pile width, and footing–pile distance show a small impact on the depth of pile bending.

The profiles of pile lateral pressure (P_L) versus depth for the same conditions discussed for the profiles of pile lateral deflection in Figure 4 are shown in Figure 8. Similar to the pile

deflection profiles, the pressure profiles have different trends between depths of 0.0 and 7.0 m depending on the pile width and footing–pile distance, while the pressure profiles are very close to each other below a depth of 7.0 m. All profiles show an increase from approximately zero lateral pressures at the top to peak values at approximately 2.0 m depth due to the footing pressure, and then, the pressures decrease to a minimum value before they gradually increase with depth, followed by the influence of the geostatic stress. For a constant footing–pile distance (B_{fp}) of 0.914 m in cases (a) and (c) and between depths of 0.0 and 7.0 m (Figure 8), the pile pressures show a drastic increase at 2.0 m depth, followed by a sharp decrease to negative values at a depth of 2.5 m. The negative portions of the pressure profiles might be the result of the combination of the large pile deflection due to the nearby footing pressure and the unit cohesion, c , of kaolin soil. In these two cases, the increase in pile width (B_p) from 0.254 to 0.356 m increases the peak pressure at 2.0 m depth from 90 to 130 kPa due to a better support from a larger pile. As the footing moves away from the pile–wall from 0.914 to 2.742 m with a constant pile width (B_p) of 0.356 m, as shown in cases (c) and (d) in Figure 8, the peak lateral pressure drops from 130 to 10 kPa at 2.0 m depth due to the lesser influence of the footing. In cases (b) and (d) in Figure 8, the pressure profiles look almost identical regardless of the pile width which reveals that, as the footing moves away from the wall, the influence of the pile width on the interaction behavior also reduces.

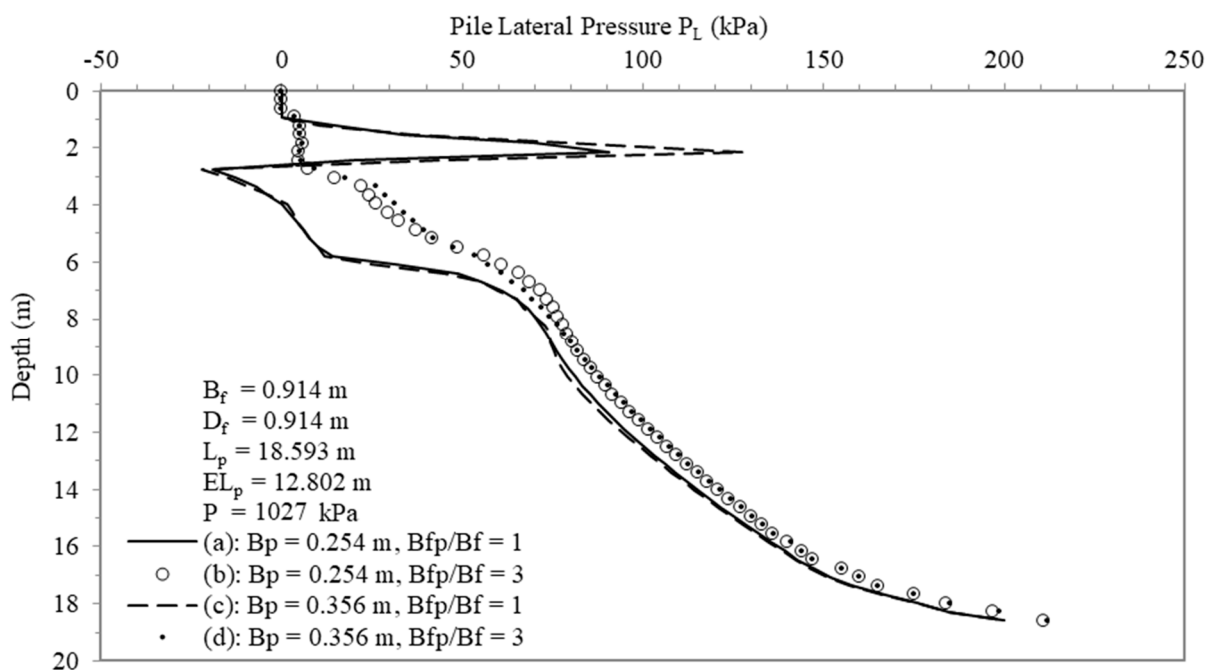


Figure 8. P_L versus depth profiles of pile-wall adjacent to strip footings resting on kaolin soil.

The profiles of pile lateral pressure (P_L) versus depth for the same conditions discussed for the profiles of pile lateral deflection in Figure 6 are shown in Figure 9. Some similarities in the general shapes of the pressure profiles between Figures 8 and 9 are shown. The peak lateral pressures at a depth of 2.0 m due to footing pressure appear to be smaller for conditions with a smaller footing shape ratio and/or longer footing–pile distance, which is expected, where the footing shape ratio (L_f/B_f) has a greater influence than the footing–pile distance (B_{fp}). The rapid increase in pressure between depths of 5.0 and 6.5 m is attributed to the less influence of footing pressure, an increase in geostatic stress, and pile bending as shown in Figure 6.

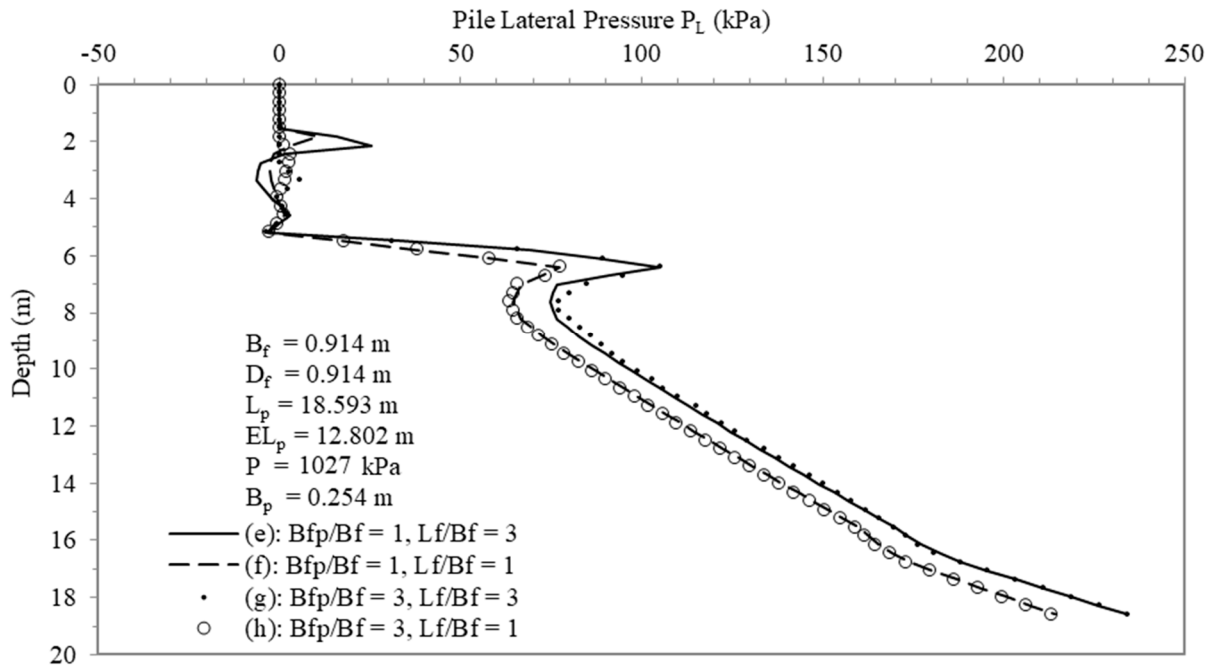


Figure 9. P_L versus depth profiles of pile-wall adjacent to rectangle and square footings resting on kaolin soil.

The profiles of pile lateral pressure (P_L) versus depth for the same conditions discussed for the profiles of pile lateral deflection in Figure 7 are shown in Figure 10. Figure 10 also exhibits a similarity in the general shapes of the pressure profiles shown in Figures 8 and 9 with minor differences at depths of 2.5 and 6.5 m due to the influence of adjacent footing pressure and pile bending, respectively. In addition, the change in soil type from silty clay to kaolin has a greater impact than the change to kaolin-sand, where lateral pressures in cases (k) and (f) drop from 35 to 10 kPa at 2.5 m depth and 120 to 80 kPa at 6.5 m depth.

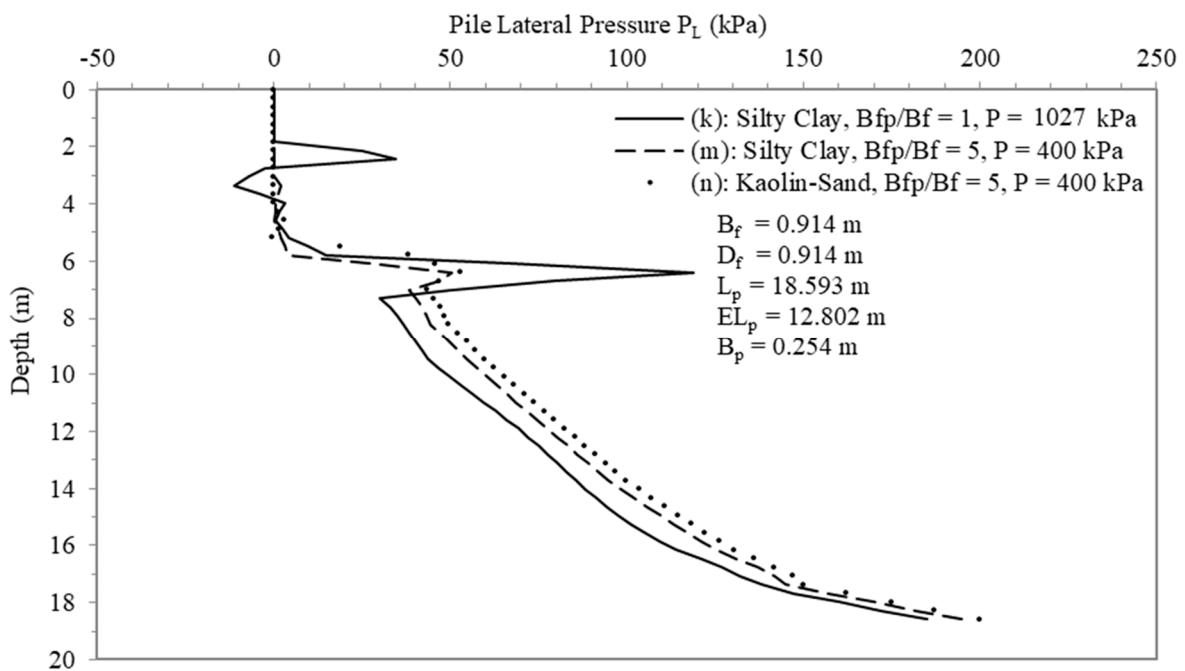


Figure 10. P_L versus depth profiles of pile-wall adjacent to square footings resting on silty clay and kaolin-sand soils.

5. Development of Pile–Wall Deflection Model

For the practical design of a pile–wall in the footing–soil–pile system (FSPS), two empirical equations are developed to predict the pile lateral deflections at the toe (δ_{LT}) and head (δ_{LH}). The predicted deflections consider the induced lateral pressure caused by the ultimate load subjected on an adjacent footing. Also, as a condition to the use of developed equations, the footing–pile distance (B_{fp}) should be equal or less than the critical distance (B_{cr}) calculated using Equation (1). These two equations are derived using multiple linear regression by Minitab 16.0 software [39]. Based upon the geometric and soil strength properties of the FSPS, eight non-dimensional terms are used as the predictors in the model: B_f/L_f , B_f/B_p , B_f/B_{fp} , B_p/B_{fp} , $\gamma B_f/c$, $\gamma B_p/c$, $\gamma B_{fp}/c$, and $1/\tan \phi$. Four terms are found to be significant for predicting pile toe deflection shown in Equation (2), while six terms are found to be significant for predicting pile head deflection shown in Equation (3). Terms with a p -value less than 0.05 are omitted from the regression results, as recommended by Montgomery et al. [40]. The values of adjusted R-squared, R-Sq (adj), are 94.3% and 86% for Equations (2) and (3), respectively.

$$\frac{B_p}{\delta_{LT}} = -72.42 + 176.65 \frac{\gamma B_f}{c} + 177.25 \frac{\gamma B_p}{c} - 24.24 \frac{\gamma B_{fp}}{c} + 13.51 \frac{1}{\tan \phi} \quad (2)$$

$$\frac{B_p}{\delta_{LH}} = -27.73 + 28.77 \frac{B_f}{L_f} - 44.73 \frac{B_p}{B_{fp}} + 46.45 \frac{\gamma B_f}{c} + 77.48 \frac{\gamma B_p}{c} - 7.35 \frac{\gamma B_{fp}}{c} + 3.38 \frac{1}{\tan \phi} \quad (3)$$

where δ_{LT} = lateral deflection of pile toe; δ_{LH} = lateral deflection of pile head; B_p = pile width; γ = wet unit weight of soil; c = unit cohesion of soil; B_f = footing width; L_f = footing length; B_{fp} = footing–pile distance, which is equal or less than the critical distance (B_{cr}); and ϕ = internal friction angle of soil. All terms in Equations (2) and (3) are non-dimensional; therefore, the units used must be consistent in each term. The ultimate load (q_u) subjected on the adjacent footing is calculated using the empirical equation developed by Sudani et al. [20], as shown in Equation (4).

$$\frac{q_u}{Q_u} = 1.0409 + 0.0949 \frac{B_f}{L_f} - 0.2821 \frac{B_f}{B_{fp}} + 0.5529 \frac{B_p}{B_{fp}} - 0.5961 \frac{\gamma B_f}{c} + 0.0761 \frac{\gamma B_{fp}}{c} - 0.0126 \frac{1}{\tan \phi} \quad (4)$$

where Q_u = ultimate bearing capacity of footing without adjacent pile–wall, which is calculated by any approved (classical) equation for an individual footing.

The relationships between the observed values, which are generated by three-dimensional finite element analysis, and the predicted values, which are generated by Equations (2) and (3), for the lateral deflections of the pile toe and head are shown in Figures 11 and 12, respectively. Figures 11 and 12 show a considerable agreement between each one of Equations (3) and (4) and the finite element analysis results.

The maximum deflection at the pile head and net pile deflection, calculated from subtracting the lateral deflections at the pile head and toe using Equations (2) and (3), respectively, are useful for the geotechnical and structural design of a pile–wall. The use of Equations (2) and (3) are recommended only within the range of variables and parameters covered in this study, which are shown in Tables 1 and 2 and Figure 1. Therefore, any extrapolation of applying data out of the range analyzed in this study into Equations (2) and (3) might not give safe results. In addition, the limitations of the present study should be considered for the applicability of these two empirical equations.

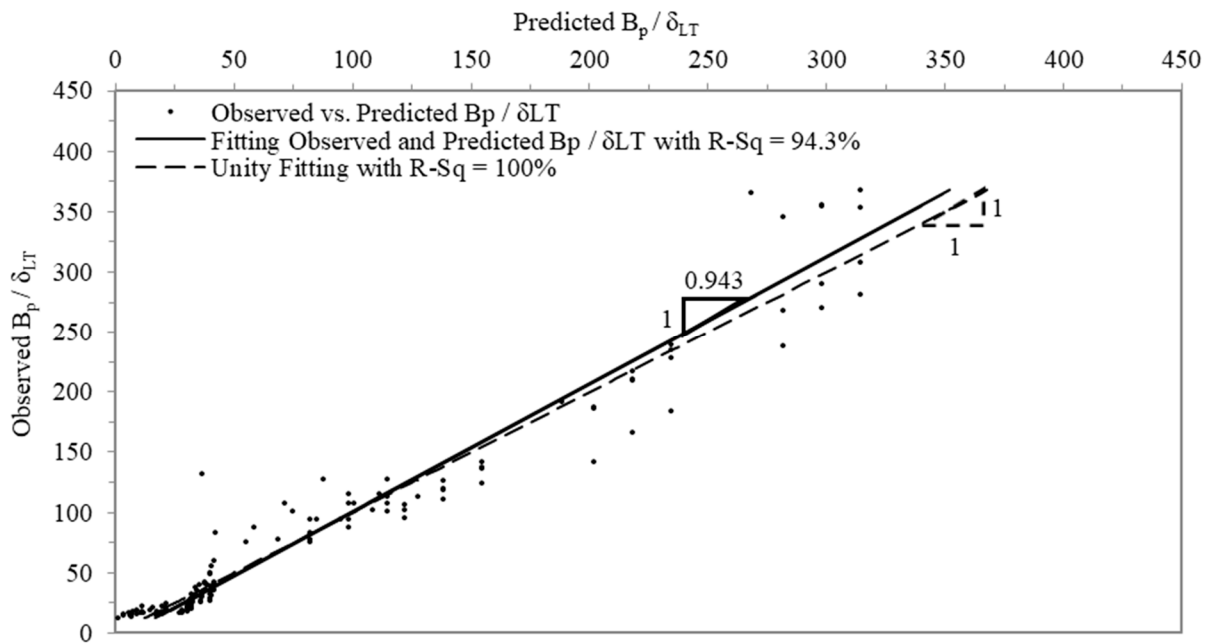


Figure 11. Relationship between observed and predicted B_p/δ_{LT} .

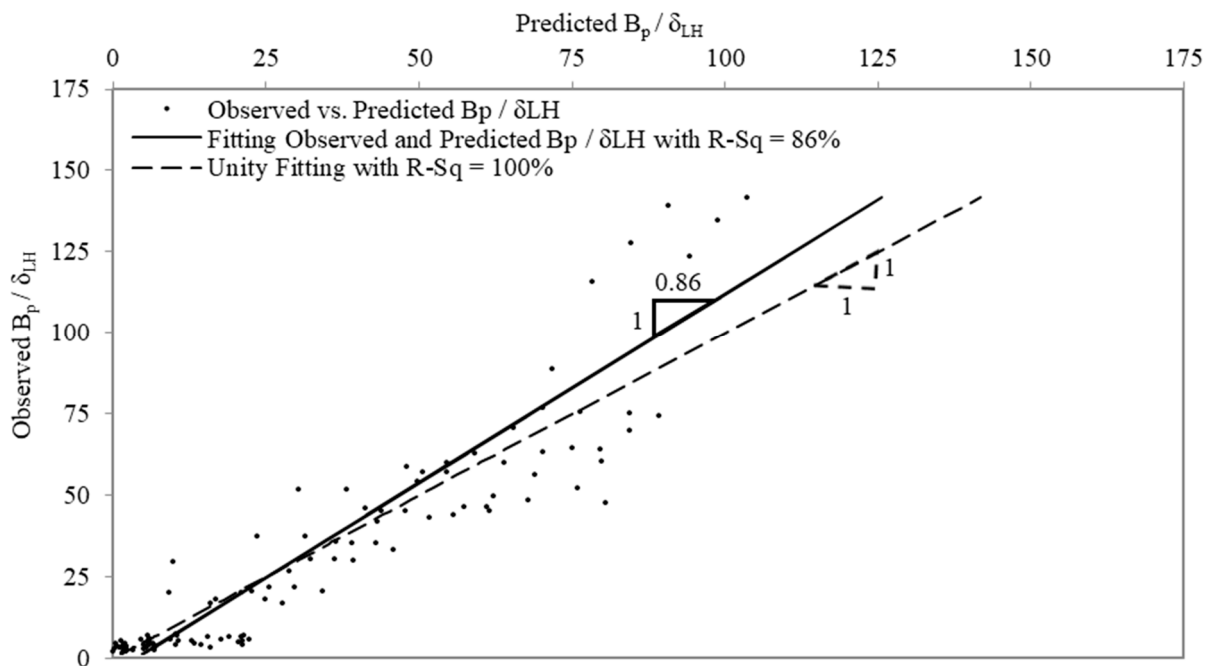


Figure 12. Relationship between observed and predicted B_p/δ_{LH} .

6. Conclusions

Based on the model results presented in this study, the following conclusions are drawn:

- (1) Lateral deflection of a pile–wall is over-estimated by more than 400% using two-dimensional (plane strain) finite element analysis in comparison with three-dimensional finite element analysis due to a lack of consideration of pile spacing and small shape ratios of adjacent footings. This issue is addressed by considering the out-of-plane geometries of a pile–wall and adjacent footing using three-dimensional finite element analysis. However, both two- and three-dimensional finite element analyses show a close prediction for the lateral deflection of the pile–wall portion below 8.0 m depth due to the small influence of adjacent footing.

- (2) Lateral deflection of the pile head decreases with increasing soil initial modulus in compression, footing–pile distance, and pile width, as well as with decreasing footing shape ratio. However, based on the results of three-dimensional finite element analysis, footing–pile distance and pile width have a small influence on the lateral deflection at the pile toe, while soil type and footing shape ratio have a greater influence on the pile toe deflection.
- (3) Due to the influence of the adjacent footing, the peak lateral pressure of the pile at the depth of approximate 2 m decreases with decreasing footing shape ratio and pile width and increasing footing–pile distance.
- (4) Based on the observed profiles of lateral pressure and deflection of pile–walls, the factors influencing the performance of a pile–wall are ranked as follows: soil type, footing shape ratio, footing–pile distance, and pile width.
- (5) Long piles tend to deflect and bend laterally rather than rotate. They also minimize the influence of footing–pile distance and pile width on the pile toe deflection. Depths of pile bending along long piles are related to the pile embedment lengths and not influenced by soil type, footing shape ratio, footing–pile distance, and pile width.
- (6) Two empirical equations are developed to predict the lateral deflections at the pile toe and head for a pile–wall located within the critical distance from an adjacent footing. These two equations are useful for the structural design of a pile–wall by providing the net deflection along a pile–wall. Values predicted using the present developed equations are in agreement with those values generated using the present three-dimensional finite element analysis. It should be noted that the present empirical equations are applicable only within the range of conditions covered in this study.

Author Contributions: Writing—original draft preparation, G.A.S.; writing—review and editing, M.J. and G.A.S. All authors have read and agreed to the published version of the manuscript.

Funding: This research received no external funding.

Institutional Review Board Statement: Not applicable.

Informed Consent Statement: Not applicable.

Data Availability Statement: The data are contained within the present article.

Conflicts of Interest: The authors declare no conflicts of interest.

References

1. Coulomb, C.A. *Essai sur une Application des Règles de Maximis et Minimis Auelques Problèmes de Statique, Relatifs a l'Architecture*; Imprimerie Royale: Paris, France, 1776. (In French)
2. Rankine, W. On the Stability of Loose Earth. *Philos. Trans. R. Soc. Lond.* **1857**, *147*, 9–27.
3. Coduto, D.P. *Foundation Design: Principles and Practices*, 2nd ed.; Prentice-Hall, Inc.: Hoboken, NJ, USA, 2001.
4. Bell, A.L. The Lateral Pressure and Resistance of Clay and the Supporting Power of Clay Foundations. In *Minutes of the Proceedings of the Institution of Civil Engineers*; ICE Publishing: London, UK, 1915; pp. 233–272.
5. Terzaghi, K.; Peck, R.B.; Mesri, G. *Soil Mechanics in Engineering Practice*, 3rd ed.; John Wiley and Sons, Inc.: New York, NY, USA, 1996.
6. Goh, A.T.; Phoon, K.K.; Kulhawy, F.H. Reliability Analysis of Partial Safety Factor Design Method for Cantilever Retaining Walls in Granular Soils. *J. Geotech. Geoenviron. Eng.* **2009**, *135*, 616–622. [[CrossRef](#)]
7. O'Rourke, T.D.; Jones, C.J.F.P. Overview of Earth Retention Systems: 1970–1990. In *Proceedings of the Conference of Design and Performance of Earth Retaining Structures*, New York, NY, USA, 18–21 June 1990; pp. 22–51.
8. Teng, W.C. *Foundation Design*; Prentice-Hall, Inc.: Upper Saddle River, NJ, USA, 1962.
9. Das, B. *Principles of Foundation Engineering*, 7th ed.; Global Engineering/Cengage Learning: Stamford, CT, USA, 2011.
10. Li, R.-P. Stability Analysis of Cutting Slope Reinforced with Anti-slide Piles by FEM. In *Proceedings of the Slope Stability, Retaining Walls, and Foundations*, Changsha, China, 3–6 August 2009; pp. 166–173.
11. Duncan, J.M.; Glough, G.W.; Ebeling, R.M. Behavior and Design of Gravity Earth Retaining Structures. In *Proceedings of the Conference of Design and Performance of Earth Retaining Structures*, New York, NY, USA, 18–21 June 1990; pp. 251–277.
12. Handy, R. The Arch in Soil Arching. *J. Geotech. Eng.* **1985**, *111*, 302–318. [[CrossRef](#)]

13. Jiang, J.; Qi, B.; Zhou, J.; Zeng, Q. Model Test and PFC2D Numerical Analysis on Soil Arching Effects Surrounding Passive Laterally Loaded Piles. In Proceedings of the Soil Behavior and Geo-Micromechanics, Geotechnical Special Publications (GSP) 200, Shanghai, China, 3–5 June 2010; pp. 240–246.
14. Jarquio, R. Total Lateral Surcharge Pressure due to Strip Load. *J. Geotech. Eng.* **1981**, *107*, 1424–1428. [[CrossRef](#)]
15. Smith, G.N.; Smith, I.G. *Elements of Soil Mechanics*, 7th ed.; Blackwell Science, Inc.: Malden, MA, USA, 1998.
16. Wang, Z.; Liu, X.; Wang, W. Calculation of Nonlimit Active Earth Pressure against Rigid Retaining Wall Rotating about Base. *Appl. Sci.* **2022**, *12*, 9638. [[CrossRef](#)]
17. Dang, F.; Wang, X.; Cao, X.; Gao, J.; Ding, J.; Zhang, L. Calculation Method of Earth Pressure Considering Wall Displacement and Axial Stress Variations. *Appl. Sci.* **2023**, *13*, 9352. [[CrossRef](#)]
18. El Sawwaf, M. Strip Footing Behavior on Pile and Sheet Pile-Stabilized Sand Slope. *J. Geotech. Geoenviron. Eng.* **2005**, *131*, 705–715. [[CrossRef](#)]
19. Sudani, G.A. Stability of Footings Adjacent to Spaced Pile-Row. Master's Dissertation, Lamar University, Beaumont, TX, USA, 2013.
20. Sudani, G.A.; Brake, N.; Jao, M. Stability of Footings Adjacent to Pile Walls. *ASCE Int. J. Geomech.* **2015**, *15*, 04015006. [[CrossRef](#)]
21. Jao, M.; Ahmed, F.; Sudani, G.; Nguyen, T.T.M.; Wang, M.C. Interaction between Strip Footings and Sheet Pile Walls. *Elec. J. Geotech. Eng.* **2017**, *22*, 1655–1674.
22. Aparna; Samadhiya, N.K. Evaluation of Model Sheet Pile Wall Adjacent to a Strip Footing—An Experimental Investigation. *Int. J. Geotech. Eng.* **2019**, *14*, 828–835. [[CrossRef](#)]
23. Azzam, W.R.; Elwakil, A.Z. Performance of Axially Loaded-Piled Retaining Wall: Experimental and Numerical Analysis. *ASCE Int. J. Geomech.* **2016**, *17*, 04016049. [[CrossRef](#)]
24. Ter-Martirosyan, A.Z.; Vanina, Y.V. A Mathematical Analysis of the Stress Statement of the Soil Basis under Complex Loading near the Retaining Wall. *Axioms* **2023**, *12*, 536. [[CrossRef](#)]
25. Fan, X.; Xu, C.; Liang, L. Experimental and Theoretical Study for a Displacement-Controlled Design Method of Embedded Cantilever Retaining Walls (Piles). *Sustainability* **2023**, *15*, 9831. [[CrossRef](#)]
26. Eilat, T.; Mitelman, A.; McQuillan, A.; Elmo, D. A Comparative Study of Embedded Wall Displacements Using Small-Strain Hardening Soil Model. *Geotechnics* **2024**, *4*, 309–321. [[CrossRef](#)]
27. ANSYS13.0. *Help System//Mechanical APDL*; SAS IP, Inc.: Canonsburg, PA, USA, 2010.
28. Drucker, D.; Prager, W. Soil Mechanics and Plastic Analysis in Limit Design. *Q. Appl. Math.* **1952**, *10*, 157–165. [[CrossRef](#)]
29. Badie, A. Stability of Spread Footing Supported by Clay Soil with an Underground Void. Ph.D. Thesis, The Pennsylvania State University, State College, PA, USA, 1983.
30. Baus, R.L. The Stability of Shallow Continuous Footings Located above Voids. Ph.D. Thesis, The Pennsylvania State University, State College, PA, USA, 1980.
31. Azam, G. Performance of Strip Footing on Two-Layer Soil Deposit with Void. Master's Thesis, The Pennsylvania State University, State College, PA, USA, 1988.
32. Baus, R.L.; Wang, M.C. Bearing Capacity of Strip Footing above Void. *J. Geotech. Eng.* **1983**, *109*, 1–14. [[CrossRef](#)]
33. Badie, A.; Wang, M.C. Stability of Spread Footing above Void in Clay. *J. Geotech. Eng.* **1984**, *110*, 1591–1605. [[CrossRef](#)]
34. Azam, G.; Hsieh, C.W.; Wang, M.C. Performance of Strip Footing on Stratified Soil Deposit with Void. *J. Geotech. Eng.* **1991**, *117*, 753–772. [[CrossRef](#)]
35. Azam, G. Stability of Shallow Continuous Footings Supported by Two-Layer Soil Deposits with an Underground Void. Ph.D. Thesis, The Pennsylvania State University, State College, PA, USA, 1990.
36. Bowles, J. *Foundation Analysis and Design*, 5th ed.; McGraw-Hill Co., Inc.: New York, NY, USA, 1996.
37. Som, N.; Das, S. *Theory and Practice of Foundation Design*; Prentice-Hall of India: New Delhi, India, 2003.
38. Tomlinson, M.; Woodward, J. *Pile Design and Construction Practice*, 5th ed.; Taylor & Francis Group: New York, NY, USA, 2008.
39. Minitab16.0. *Help Manual*; Minitab, Inc.: State College, PA, USA, 2010.
40. Montgomery, D.; Runger, G.; Hubele, N. *Engineering Statistics*; John Wiley and Sons, Inc.: New York, NY, USA, 2011.

Disclaimer/Publisher's Note: The statements, opinions and data contained in all publications are solely those of the individual author(s) and contributor(s) and not of MDPI and/or the editor(s). MDPI and/or the editor(s) disclaim responsibility for any injury to people or property resulting from any ideas, methods, instructions or products referred to in the content.